Babes-Bolyai University
Faculty of Physics

STRUCTURAL INVESTIGATIONS OF MOLECULAR COMPLEXES WITH BIOLOGICAL INTEREST

Phd thesis summary

Scientific supervisor :
Prof. Dr. Leontin David

Phd student:
Mare Daniela Aurica

2012

The contents of the thesis

INTRODUCTION

In recent years research in physics, chemistry and medicine focuses on the synthesis and characterization of biological compounds containing metal ions in living organisms because they fulfill important functions that ensure their proper functioning. Vegetable and animal bodies are made up of chemicals both metal and non-metals.

In most metal ions that are found in the body are in the form of complexes or their acting within the training complex, usually chelates. They are stable in terms of power, protecting metal reactions physicochemical occurring during digestion in the body..

Studies on transition metal complexes with the ligand molecules of biological interest showed an increase in their molecular activity compared with pure ligands. The biological activity of the complexes is dependent on the local structure around the metal ions, and the type and strength of chemical bonds. Polyoxometalates are a class of coordination compounds by polycondensation oxoanionilor resulting metals and non-metallic elements oxoanioni various .In recent years polyanions derived from metals especially in the transition to adopted the name of polyoxometalates, namely iso polyoxometalates and heteropolyoxotungstates.

The most intensively studied application refers to the biological activity of many species heteropolyoxometalates used especially in medicine as antiviral agents, anticancer, antienzimatici, coagulants and anticoagulants. Also studies have shown Keggin type polyoxometalates their effectiveness against herpes type viruses, human immunodeficiency viruses type 1 and type 2 (HIV) . Literature has numerous studies on a new class of anionic ligands that inhibit HIV replication.

The present work ,entitled" ***Structural investigations of molecular complexes with biological interest"*** the contribution they make to various physico-chemical (elemental chemical analysis, atomic absorption), heat (thermogravimetry, differential scanning calorimetry) and spectroscopic (FT-IR spectroscopy, UV-VIS, EPR, EPR) to determine the biological activity of complexes metal. The thesis is structured in five chapters as follows:

The first chapter entitled: „***Transition metals, biologically activity and physico-chemical properties of metal complexes and molecular complexes heteropolyoxometalates "*** presents role, activity, physical and chemical properties of metals and metal complexes.Has also presented polyoxometalate properties and classification. The second chapter ,entitled „***The experiments techniques for investigating metal complexes "*** presents different spectroscopic methods (FT-IR, UV-Vis, ESR, Raman) and qualitative and quantitative chemical analysis of the molecular structure of metal complexes. The third chapter,entiled

„***Study of metal complexes of Cu^{2+} with ligands sulfonamides*** **"**presents synthesis and characterization of new metal complexes of $Cu^{2+}$by *[Cu (L)$_2$($C_6H_4N_2$) (H_2O)]* and *[Cu_2(L)(OH)$_2$ (C_3H_7NO) (H_2O)] (H_2O)* where the ligand is HL = *N-(5-ethyl –[1,3,4]-thiadiazole-2-yl)-toluenesulfonamidate]* through methods FTIR ,SERS . Sulfonamides drugs were the first antimicrobial drugs that prevent the growth of bacteria in the body and have paved the way for new antibiotics in medicine.

The fourth chapter ,entitled „***Vibrational spectroscopic studies on paroxetine molecule "*** structural results are obtained by vibrational spectroscopic methods (FTIR, Raman şi SERS), and the functional theory calculations based on density (DFT) performed on paroxetine molecule (3S,4R) - 3 - [(1, 3 - benzodioxol - 5 - iloxi) metil] - 4 - (4-fluorofenil) piperidină, a medicine used to treat depression, panic and social anxiety. After the to our data, assigning normal modes of vibration of paroxetine IR and Raman spectroscopy on coupled quantum chemistry calculations have been made.

The last chapter ,entitled ***„Spectroscopic studies of new Keggin polyoxometalates "*** following summarizes polyoxometalates $K_6[Mn(H_2O)PVMo_{10}O_{39})]\cdot 10\ H_2O$, K_5 [Fe (H_2O) $PVMo_{10}O_{39}] \cdot 8H_2O$, $K_6[Co(H_2O)PVMo_{10}O_{39}]\ 22H_2O$, K_6 [Ni (H_2O) $PVMo_{10}O_{39}] \cdot 21H_2O$, K_6 [Cu (H_2O) $PVMo_{10}O_{39}] \cdot 17H_2O$.

Practical applicability of their compleccşilor metal polyoxometalate and manifests in different fields as catalysis, medicine, pharmacy, chemistry, material science which are used for new hybrid molecular materials, or their high selectivity at inhibiting enzymes.

The obtained results will be able to find a recent and similar promising application in medicine and pharmacy.

Keywords: *FT-IR spectroscopy, UV-VIS spectroscopy, ESR spectroscopy, Keggin-type polyoxometalate, transitional metal, Raman-SERS spectroscopy, dimethylformamide, phenantroline, paroxetine,* heteropolyoxometalates, monolacunary polyoxometalate, thyadiazol, *N-substituted sulfonamides.*

1. TRANSITION METALS, BIOLOGICALLY ACTIVITY AND PHYSICO-CHEMICAL PROPERTIES OF METAL COMPLEXES AND MOLECULAR COMPLEXES HETEROPOLYOXOMETALATES

1.1. The biological role of the transitional metals

Of all known chemical elements in the composition of living matter are about 52. Mainly occur in living organisms bioelements 40-43, 25 are essential for the structure and functionality, among which C, N, H, O, P, S which is based on building living organic matter (protein, glycogen, starch, lipids and nucleic acids) [1].

1.2. The biological activity of the metal complexes

Transition metal chemistry $(n-1)d^{1-10}ns^2$, where n =4, 5, 6, 7, property is dominated by atoms or ions to form their many complex combinations presenting a wide variety of structures. Chemical reactivity of transition elements d depends on the nature of the metal, and the state it is: compact or finely divided, temperature, pressure, atmospheric composition and the presence of pollutants. Transition metal ions are paramagnetic atoms like them.

1.3.Physical and chemical properties of metal complexes

The combinations underlying complex biological processes, as well as the coordination catalitice.Compuşii reactions are generally combinations containing a central atom or ion (usually a metal) surrounded by a number of ions or neutral molecules. Depending on the amount of load central ion and groups that surrounds him, can be a complex combination of cation, anion or neutral molecule. These combinations tend to maintain their identity even in solution, although in some cases it may be a dissociation.

There are many criteria for the classification of coordination compounds, however, the classification of coordination compounds can be made by: the nature and number of atoms (ions) generated by complex coordination spheres respectively, coordination number, oxidation number generator complex type ligands in the coordination sphere. They are turn are divided into: classics Werner- Miolat type compounds, metal chelates, organometallic compounds coordination compound , metal carbonyls, encrypt cluster, iso- and heteropolicompounds, moleculars. [2]

Ligands classification is based on: the nature of the donor atom through which the ligand binds to the metal ion, the number of donor atoms of the ligands, ligands task. Coordination numbers can be between 2 and 12, the most common being 4 and 6. Metallic

ions in biological systems usually form compounds with coordination numbers 4, 5, 6 and 8. Compounds with other biological ion coordination numbers are unstable, they generally represent intermediate stages in the development of biological processes.

1.4. Classification and properties of complexes of polyoxometalates

Polyoxometalates– class of inorganic compounds, coordination, resulting in polycondensation oxoanyons macromolecular-metal and non-metallic elements with identical oxoanyons (isopolyoxometalates) or different (heteropolyoxometalates) [3,4].

Heteropolyoxometalates as ligands can form complex combinations, their classification is done according to several criteria (adenzi chemical identity of atoms, the electronic structure of heteroatoms primary oxidation state of atoms addent).

1.4.1. Heteropolyoxometalates completely saturated.

HPOM formation involves polymerization of polyhedra around heteroatoms primary training when the solution has an acidic, leading to the formation of high molecular weight rigid structures. Arrangements also are relatively stable thermodynamically kept their identity in aqueous and non-aqueous solutions, as in ionic crystals.

From studies on a series of complex combinations of very large HPOM revealed that their heating takes place by gradual loss of water molecules, molecules that play an important role in stability, by decomposing HPOM. HPOM crystals generally have a lower energy network, but change in ion transition metals are incorporated active centers for reduction reactions.

1.4.2. *Heteropolyoxometalates defective*

Is obtained by removing the complete structure of an atom addendum with terminal oxygen atom coordinated to it or two or more such links ($M=O_d$)

Incomplete fragments are either stable or unstable after their formation in solution. For stabilization, these fragments can be coupled into dimers structures, trimmers or tetramere.

2. THE EXPERIMENTAL INVESTIGATION TECHNIQUES A METAL COMPLEXES

This chapter aims to show generally that the origin of all spectra are interactions between substances and electromagnetic waves. General elements of the spectrum and structure of this chapter are reproduced specifically for each type of compound investigated in the following chapters.

2.1. The qualitative and quantitative chemical analysis

Analytical chemistry is the basis of chemical analysis methods, methods that can be defined as a set of principles and processes that can identify and possibly dispensing components of the sample. Analytical methods of analysis are characterized by accuracy, precision, sensitivity, precision and selectivity. Principle of a method quantitative determination of chemical elements is high temperature combustion of solid or liquid samples in oxygen atmosphere in the confined space. Thus, elemental chemical analysis enables the formula and molecular mass and elemental analysis for determining the molecular formula of the compound.

2.2. The Atomic absorption spectroscopy and thermal gravimetric

Atomic absorption spectrometer measures the radiation absorbed by atoms which remain fundamental (neexcitați) gas. Their number is usually much larger than the excited atomic absorption spectrometry is a method characterized by a much better sensitivity, at least until temperatures by 5000K.

Differential thermal analysis is an analysis technique where the temperature difference between a sample and a reference material is measured as a function of sample temperature through the sample is measured with increasing temperature [8]. The method is useful in determining sample purity and concentration of water, carbonates or organic substances in materials, but generally for studying any thermal decomposition reactions. Recorded mass changes lead to some graphics called thermograms or thermogravimetric curves (TG), as well as their differential thermogravimetric analysis differential called (DTG).

2.3.Electronic spectroscopy UV-Vis

In the ultraviolet and visible spectroscopy is based on absorption of radiation by molecules in these areas, resulting absorption transition of electrons from orbitals σ, π or in a low energy state, an excited state with higher energy.Electronic spectrum is a graphical representation of the absorption intensity depending on the wavelength of radiation that radiates elementary sample containing organic compound studied. The spectroscopy of the visible light

is provided by a tungsten source (329 nm-2500 nm) and in UV spectrometry with deuterium or hydrogen lamp (160 nm – 380 nm). [9] In UV-Vis detection and quantitative determinations are based on the measurement of transmittance or absorbance of the test solution electromagnetic radiation (light) absorbed is proportional to the analyte concentration.

2.4. The Fourier transform infrared spectroscopy (FT-IR)

Infrared wavelengths with high and low energy electronic transitions can occur but can produce vibrational and rotational transitions of molecules. To obtain spectra in the IR spectrometer is used which is set radiation absorbed by an analyte molecule, radiation disappears the complexity of the incident radiation beam. IR spectrum shows the intensity spectrum frequency $\overline{\nu}$, wave number or wavelength(λ)[10].

Band intensities can be expressed either as transmittance (T) or as absorbance (A).

2.5. Electron spin resonance (RES)

Electron spin resonance angular momentum requires the presence of a test subject in the study of spin angular momentum is due to electrons of atoms and molecules neîmperecheați studied systems and corresponding orbital orbital p, d or f of gaseous atoms or molecules. Formally, the RPE is the general name, as some systems can be paramagnetic without electronic [11].

Electron spin resonance applies to molecules containing odd electrons. Apply a fixed frequency ν electromagnetic radiation (monochromatic radiation) and vary the magnetic field B.

ESR experiment takes place generally at fixed microwave frequencies. The frequency bands used are X (~9.5 GHz) şi Q (35 GHz). [12]

ESR spectrum contains information about the intensity, line width, the factor structure of multiplet giromagnetic and parameters providing information about complex concentration, the energies of the spin states and interactions with neighboring nuclei, dynamic processes, spin-spin interactions.

2.6. The Raman spectroscopy

The Raman spectroscopy is based on vibrational transitions, intrinsic fine structure of the Raman spectra allows elucidation of molecular structure, surface processes and reactions at the interface. Raman scattering refers to light that is refracted in the direction of propagation of the incident light. The main types of scattering are Raman scattering Stokes and anti-Stokes Raman scattering. Raman scattering effect occurs when there is an exchange of energy between the photon and the molecule, which leads to the emission of another photon with a different frequency than the incident photon. [13]

3.THE STUDY METALLIC COMPLEXES CU^{2+} OF THE SULPHONAMIDES LIGANDS

3.1 Introduction

In this study we report the synthesis, crystal structure and properties of two news Cu^{2+} complexes with N-substituted heterocyclic sulfonamides: $[Cu(L)_2(phen)(H_2O)]$ (**1**) and $[Cu_2(L)(OH)_2(dmf)(H_2O)](H_2O)$[HL=N-(5-ethyl–[1,3,4]-thiadiazole-2-yl)-toluenesulfonamidate] (**2**). In the both two complexes, the Cu^{2+} ion is five-coordinated. The ligands act as monodentate, coordinating the metal ion through a single $N_{thiadiazole}$ atom. The molecule of phenantroline also participle to the coordination of Cu^{2+} ion as bidentate ligands. The physical-chemical properties of the complexes have been studied by FT-IR, electronic and EPR spectroscopic methods. [14] Sulfonamides are used to treat many types of infections caused by bacteria and microorganisms.

New sulphonamides occurred at an amazing speed had greater use, as a wider range of antibacterial and lower toxicity.

3.2. Synthesis of the Complexes

Elemental analysis indicates a combined ratio Cu(II) : ligand: dimethylformamide (dmf) of 2 : 2 : 1; phenantroline of 1 : 2 : 1. To the coordination of the metallic ion in case of dimethylformamide (dmf) also participate water molecules and OH^- ions from the reaction medium; in case of phenantroline the metallic ion is also coordinated by an H_2O molecule from the reaction medium.

Tabel 1 Elemental analysis results for **complex 1** and **2**

Complex	*Elemental analysis (%) (found/calculated)*			
	C	*H*	*N*	*S*
1	*48.27* 48.12	*3.70* 3.75	*13.98* 14.03	*16.25* 16.04
2	*34.58* 34.49	*3.96* 4.02	*12.30* 12.2	*16.09* 15.9

			2	8

For the **complex 1:** 1 mmol of HL4 ligand is dissolved in a mixture of 50 ml methanol and 10 ml dimethylformamide. Separately, a solution of 0.5 mmol $Cu(CH_3COO)_2 \cdot H_2O$ and 5 ml of water was prepared. The copper solution is added to the ligand solution under continuous stirring. The resulting mixture is stirred at room temperature for two hours. The resulting light green solution is kept in a crystallizer at room temperature.

For the **complex 2:** 1 mmol of ligand (HL) is dissolved in 40 ml of methanol which was previously mixed with 2 ml of a NaOH solution 1M. Separately, another mixture is prepared by dissolving 0.5 mmol $CuSO_4 \cdot 5H_2O$ and 0.5 mmol of phenantroline (phen) in 25 ml of methanol (a turquoise precipitate is obtained in the solution). By adding the ligand solution in the Cu(II)-phenantroline mixture, the color turns to green.

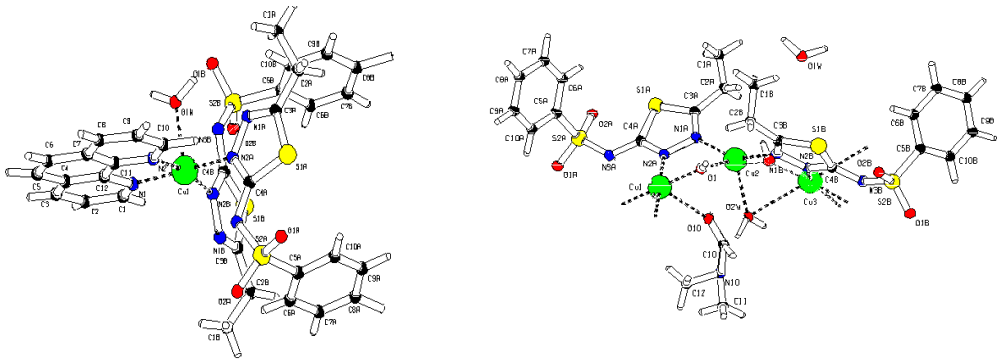

A: Complexul 1 ***B: Complexul 2***

Fig. 1.1. Crystalline structure of the **complex 1**(fig. a) and **complex 2**(fig. b)

Infrared Spectroscopy

In the IR spectrum of the **complex 1** (Fig. 2 (a)) we can see the 1518 cm^{-1}, 843 cm^{-1} and 716 cm^{-1} bands, which do not appear in the spectrum of the free ligand and which can be attributed, according to literature, to the phenantroline molecule which participates to the coordination of the metallic ion. In the IR spectrum of this complex we can also see a broad band at 3600-3300 cm^{-1} wich could be attributed at OH vibration of water molecule. All data correspond to those presented in literature for complexes with a similar structure.

The spectrum of the **complex 2** (Fig.2 (b)) shows bands at 1655 cm^{-1}, 1381 cm^{-1} and 1085 cm^{-1}, which can be attributed to the dimethylformamide which participates in the coordination of the Cu(II) ion, as they do not appear in the IR spectrum of the free ligand. The characteristic bands of the OH^- group and of the water molecule from the structure of the complex cannot be identified, as they overlap the bands of the ligand

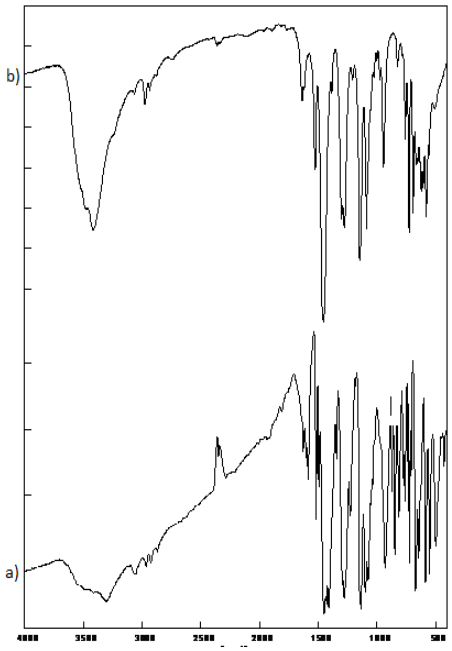

Fig.2. IR spectrum of the complex**1** (a) and complex**2** (b)

Diffuse Reflection Electronic Spectra

The electronic spectrum of the **complex 1** (Fig.3 (a)) shows a single strong band at 662 nm. This band corresponds to the d-d transitions in the Cu(II) metallic ion. This confirms the square pyramidal geometry for this complex, where the Cu(II) ion is pentacoordinated. The band at 372 nm (Fig.3 (b)) is attributed to the charge transfer from the metallic ion to the ligand or vice versa, while the more intense band at 622 nm appears due to the d-d transitions in the Cu(II) ions from the **complex 2**.

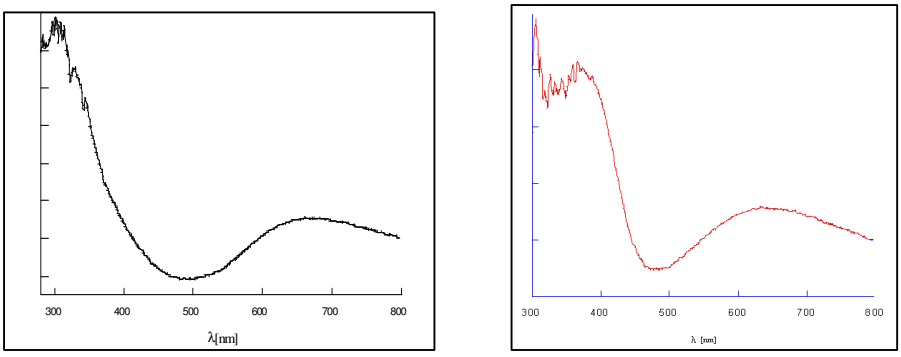

Fig 3 Diffuse UV-Vis reflection spectrum of the ***complex 1*** *(a) and* ***complex 2*** *(b)*

3.4. Conclusions partial

Metallic ions, including Cu^{2+}, and their coordinative compounds, can produce in the presence of reducing agents, reactive free radical species which can cleavage the DNA molecule. This property has spurred studies concerning their use in complexes with Fe^{2+}, Mn^{2+}, Cu^{2+} etc. ions as potential "artificial chemical nucleases". The driving force of ours research field is the development of biological tools to study DNA structure, the preparation of DNA footprinting agent, the study of the DNA oxidations and the elaboration of potential antitumoral or antiviral agents.

4. *VIBRATIONAL SPECTROSCOPIC AND DFT STUDY ON PAROXETINE MOLECULE*

4.1. General data on paroxetine

This paper presents the structural results obtained by vibrational spectroscopic methods (FTIR, Raman and SERS), and the calculations based on the functional density theory (DFT) performed on paroxetine molecule [16]. Paroxetine (trade names Seroxat, Paxil) (3S,4R) -3- [(2H-1,3- benzodioxol -5-yloxy) methyl] -4-(4-fluorophenyl) piperidine is a selective serotonin reuptake inhibitor (SSRI) antidepressant. Paroxetine is used to treat major depression, obsessive-compulsive, panic, social anxiety, and generalized anxiety disorders in adult outpatients [17-18].

Raman scattering provides important structural information on molecules and when they are adsorbed on metal surfaces (Au, Ag) Raman section is amplified by several orders of magnitude and can therefore be investigated analytes in micromolar concentration [19].

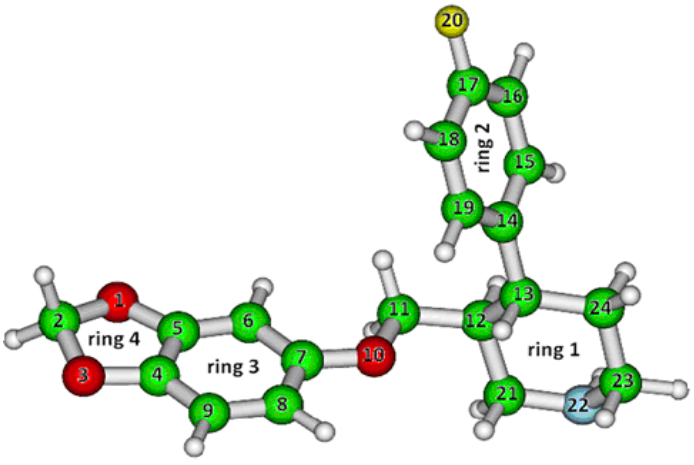

Fig. 4.1. Geometry optimized B3LYP/6-31G (d) of paroxetine

with the numbering of atoms and rings (rings)

4.2. Experimental methods for investigating the structure

Colloidal silver SERS substrate was prepared by reducing Ag + with hydroxylamine. PH, colloidal silver solution, measured immediately after preparation, was 8.5.

Vibrational frequencies were calculated at the geometry optimized to ensure that no imaginary frequency was obtained either confirming that it corresponds to a local minimum on the potential energy surface.

Experimental band assignments are based on the observed band frequencies and their intensities experimental Raman spectra and confirmed by establishing one to one correlation between the observed and theoretical frequencies calculated. For graphical representation of the calculated Raman spectrum were used forms of lines (bands) pure Lorentz width at medium height (FWHH) by 15 cm^{-1}.

Vibrational mode assignments were made by observing animated visual patterns using Molekel program [20] taking into account both band positions and intensities.

4.3. Raman and SERS Spectra

FT-Raman and SERS spectra of paroxetine are shown in Fig.4.3., and selected experimental bands SERS and FT-Raman and their wave numbers and relative intensities calculated at the level of theory B3LYP / 6-31G (d) are summarized in Table 2.2.

Mean absolute deviation between calculated and experimental Raman spectra is 11.36 cm-1, with an RMSD of 14.13 cm-1 (SD = 13.90 cm^{-1}) and normalized RMSD value of 1.05%. The largest discrepancy between theory and experiment is observed for the Raman band at 805 cm -1, corresponding to the breathing vibration of benzene rings and dioxolane. As shown in Fig.4.3., this is the most intense band in both experimental Raman spectra as well as the calculated.

FT-Raman bands at 253, 470 and 573 cm-1 is mainly due to deformations in the plane of piperidine (ring 1) and benzene (ring 2). $C_{11}H_2$ group rocking vibrations superimposed deformation occurring outside the plan inelului3 to 351 cm-1.

Breathing vibration of benzene (iring 2) and benzodioxol (ring 3 and ring 4) appear at 846 cm-1 and 805 cm-1 respectively, are quite intense in the experimental spectrum. Banda at 1197 cm-1 is due to bond elongation of piperidine and fluorophenyl rings coupled with deformation vibrations of CH groups plan to benzene (ring l2).

The calculations piperidine ring characteristic bands are observed in the Raman spectrum at 946 and 1358 cm^{-1}, while the fluorophenyl ring such bands are observed at 1197 and 1218 cm^{-1}. Bending and stretching vibrations of the benzene ring contributes significantly to the normal modes giving rise to Raman bands at 1297 and 1604 cm^{-1} and bands at 1063,

1094, 1159 and 1502 cm^{-1} are associated mainly with the vibration characteristics dioxolane ring. Thus, SERS bands most displaced are observed at 966, 1140, 333, 533, 582 and 1285 $cm^{-1.}$

4.4. IR spectra analysis

IR absorption spectra, experimental and calculated spectral range of paroxetine 600-3500 cm-1 are shown in Fig.4.2., And assigning the most intense bands is summarized in Table 3. You can also easily see in this table that the values B3LYP/6-31G (d) predicted theoretically are in good agreement with experimental values. Most intense band in the IR spectrum is observed at 1183 cm^{-1} and is excellent quantum chemistry calculations reproduced both the position and intensity.

Bands located at 765, 914 and 931 cm^{-1} are due to bending vibrations (deformation) of the piperidine ring (1) and C11H2 group. Deformation vibrations of ringului3 contribute mainly to experimental bands at 781, 835, 944, 1097, 1183, 1247 and 1279 cm^{-1}, while the corresponding normal modes ringului4 associated with experimental bands at 675 and 1381 cm^{-1}.

The benzenic ring stretching vibrations dominate more normal modes associated with bands at 1629, 1606, 1479, 1438 and 1381 cm $^{-1}$, while the fluorophenyl ring thus contributes to the normal vibration which gives rise to the band at 1502 cm $^{-1}$. Banda located at 1040 cm^{-1} is also related to vibrations of the ring plane deformation is attributed $C_2H_2O_2$ group of dioxolan ring coupled with elongations CC ring 1

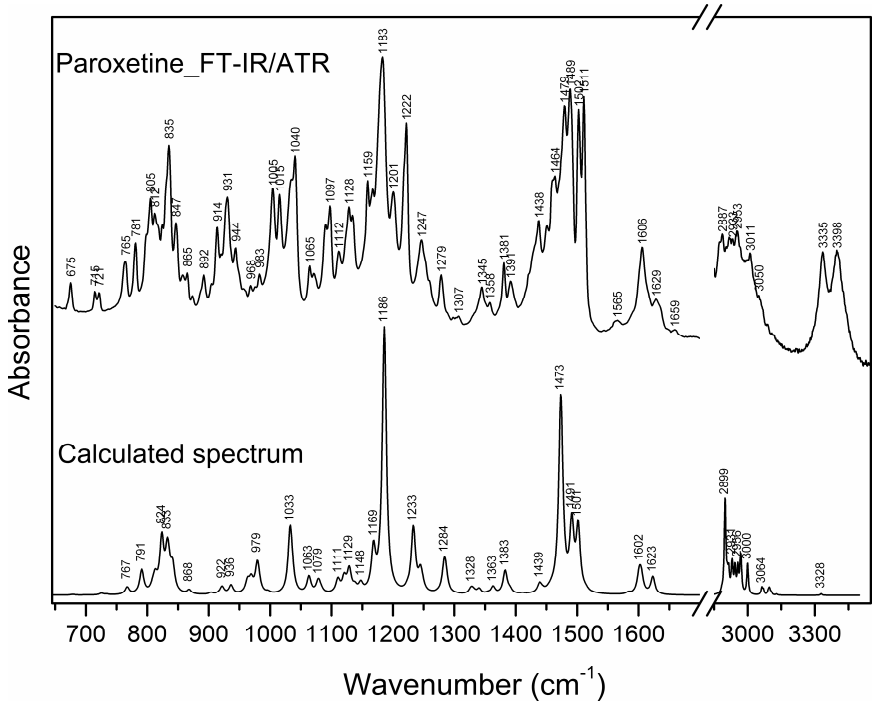

Fig. 4.2. IR spectra, experimental and calculated, of paroxetine

Table 3. Selected FTIR bands with wave numbers and IR intensities calculated

Experimental wavenumbers (cm^{-1})		**Calculated wavenumbers (cm^{-1})**		**Assignments**
FTIR/ATR	**I_{IR}**	**B3LYP**	**I**	
1	**2**	**3**	**4**	**5**
3335	40	3328	1	ν(NH)
3011	38	3000	12	$\nu_{as}(C2H_2)$
2953	44	2956	10	$\nu_{as}(CH_2$ ring2)
2933	42	2931	9	ν(CH, CH_2 ring1)
2887	44	2899	29	$\nu_s(C2H_2)$
1629	20	1623	7	ν(CC ring3)+δ(CH ring3)
1606	38	1602	7	ν(CC ring3)+δ(CH ring3)
1511	90	1514	1	$\delta(C2H_2)$
1502	86	1501	24	ν(CC ring2)+ν(CF)
1489	92	1491	25	ν(C7O10)+δ(CCC ring 3)+$\delta(C2H_2)$+δ(CH ring3)
1479	86	1473	75	ν(CC ring 3)+$\delta(C11H_2)$+δ(CH ring3)
1438	44	1439	5	ν(CC ring3)+ν(C5O1)+$\delta(C11H_2)$+$\delta(C2H_2)$
1381	28	1383	9	ν(CC ring 3)+ν(CO ring4)+$\omega(C11H_2)$
1345	18	1341	2	ν(CC ring1)+ν(CN ring 1)+ν(C11C12)+$\tau(CH_2)$
1279	22	1284	8	δ(CCC ring 3)+δ(CH ring2)
1247	34	1245	7	ν(CC ring 3)+δ(CH ring 2)+δ(CH ring 3)
1222	76	1233	18	δ(CCC ring2)+ν(CF)+$\delta(C11H_2)$+δ(CH ring1)
1183	100	1186	100	δ(CCC ring3)+ ν(CO)+$\delta(C2H_2)$+ δ(CH ring3)
1159	54	1169	15	$\delta(C2H_2)$+δ(C13H)
1128	44	1129	11	ν(CC, CN ring1)+$\rho(C11H_2)$
1097	45	1079	6	δ(CCC ring 1, ring 3)
1065	20	1063	7	δ(CCC ring 3)+ν(C11C7)+ν(CO ring 1)
1040	63	1035	5	δ(OC2O)+ν(CC ring1)
1015	48	1033	23	δ(OC2O)+ ν(CC ring1)
1005	50	996	3	δ(CCC ring 2)
944	26	963	4	δ(CCC ring 3)+δ(OCO ring 4)
931	46	936	4	$\rho(C11H_2)$+δ(CH, CH_2, NH ring1)
914	34	922	4	δ(ring1+δ(ring3)
892	16	868	2	breathing(ring2)+δ(CH, CH_2, NH ring1)

847	34	841	9	γ(CH ring 2)
835	62	833	14	γ(C6H, CH ring3)
805	42	824	20	γ(NH, CH ring1, ring2)
781	26	791	10	breathing(ring 1)+γ(NH)+δ(ring 3, ring 4)
1	**2**	**3**	**4**	**5**
765	20	767	3	δ(C14C13C24)+γ(ring1)+γ(NH)
675	10	678	1	δ(ring1,3,4)+δ(O10C11C12)
I_{IR}-FTIR intensity, I-Intensity, ν- stretch, ν_s- symmetric stretch, ν_{as}- asymmetric stretch, δ- in plane bending, ρ- rocking, τ-twisting, ω-wagging, γ-out of plane bending, ip.-in plane, ring1: piperidine ring (N22-C21-C12-C13-C24-C23); ring2: fluorophenyl ring (C14-C15-C16-C17-C18-C19); ring3: benzene ring (C4-C5-C6-C7-C8-C9); ring4: dioxolane ring (O1-C2-O3-C5-C4)				

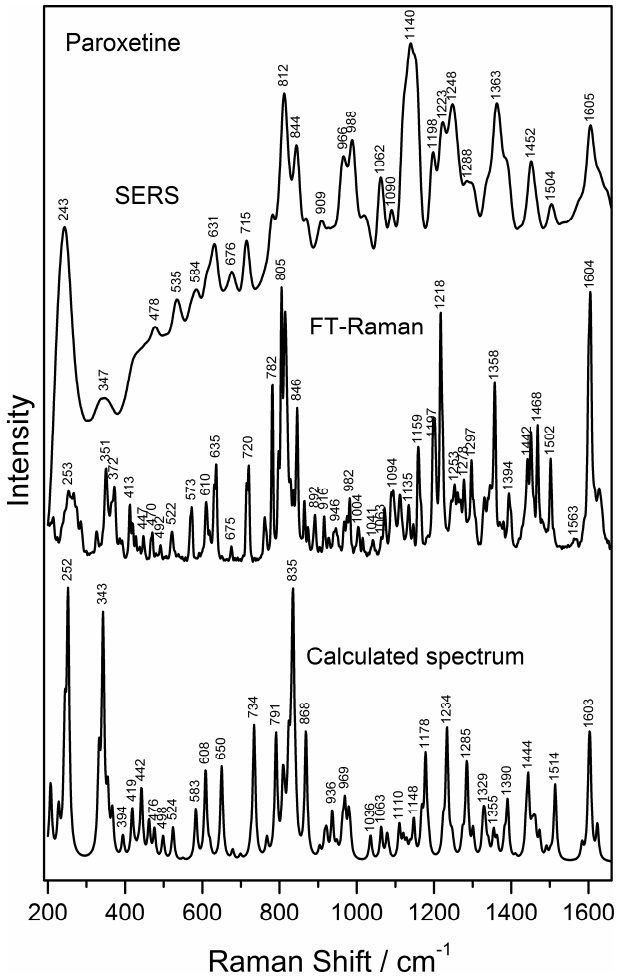

Fig.4.3. SERS spectra, FT-Raman and calculated Raman of paroxetine

SERS band at 966 cm^{-1} is shifted to the blue by 20 cm^{-1} corresponding mainly elongation of the ring CC 1. She is also enhanced, thus providing clear evidence for the existence of strong interactions between inelul1 silver surface. Strong interaction between ring 1 and silver surface is also supported bands shift to 533 and 582 cm^{-1}, both of which shifted by 11 cm^{-1} and 9 cm^{-1}. Involvement ring 3 in adsorption is supported by the SERS banda 1288 cm^{-1} (ν(CC)ring 3), redshifted by 9 cm^{-1} from the FT-Raman spectrum and the SERS band at 347 cm^{-1}, shifted from 351 cm^{-1} in FT-Raman spectrum corresponding to a mode containing vibration out of plane ring 3. As can be seen in the map molecular electrostatic potential (MEP) of paroxetine molecule (***Fig.4.4.***) obtained from DFT calculations, the negative charge is mainly located on the oxygen atoms (O1, O3, O10) and nitrogen atom (N22) of piperidine.

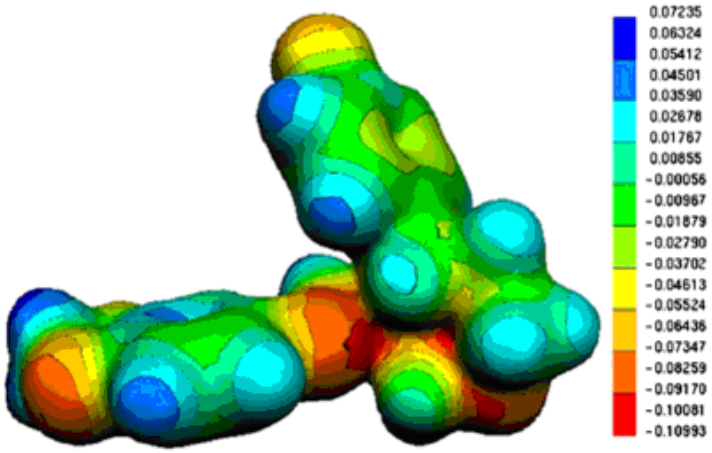

Fig.4.4. 3D electrostatic potential calculated at B3LYP/6-31G (d) for paroxetine (u) represented izosuprafața the electron density of 0.02 AU

Consequently paroxetine adsorption on the surface of silver nanoparticles in colloidal solution must take place through three oxygen atoms and one nitrogen. This is illustrated by the appearance of intense band at 243 cm^{-1} in SERS spectra characteristic vibrations Ag-O and Ag-N, with no counterpart in normal Raman spectrum. In order to simulate the interaction of the molecule with the silver surface we optimized two complexes formed between paroxetine molecule and a Ag atom located in close proximity to the N22 atom or molecule near the dioxolane ring. Wave numbers obtained are 244 cm^{-1} for Ag-N vibration and 226 cm^{-1} for Ag-O vibrations. Consequently banda from 243 cm^{-1} is certainly the result of interaction Ag-N22.

Intense SERS band at 812 cm-1 is due benzodioxol ring breathing vibration (ring 3 + ring 4) adsorbed in a tilted orientation in the vicinity of the silver surface, as illustrated in ***Fig. 4.5.***

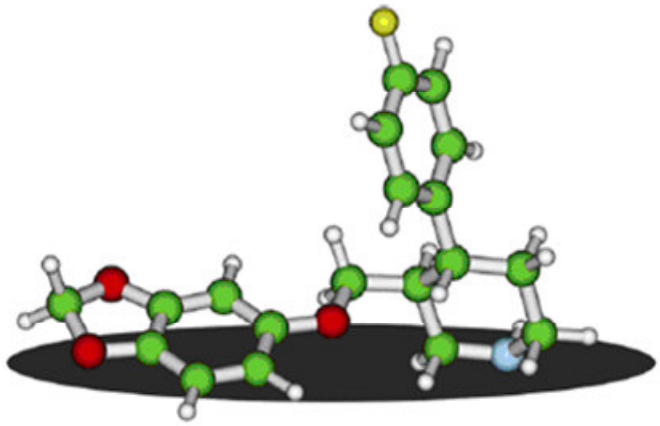

Fig. 4.5. Adsorption geometry of the molecule on the surface of paroxetine silver nanoparticles

SERS band at 1605 cm-1, attributed to CC elongation and bending vibrations of CH groups plan the The benzenic ring (inel3) also supports this hypothesis [27].

Breathing vibration of The benzenic ring (inel2) shows a band of medium intensity resulting from the orientation perpendicular to the silver surface as SERS selection rules [28].

Table 4. A selection of SERS and FT-Raman bands with wave numbers and Raman intensities calculated for paroxetine.

Experimental wavenumbers (cm^{-1})				**Calculated wavenumbers cm^{-1})**		**Band assignment**
SERS	**I_S**	**FT-Raman**	**I_R**	**B3LYP**	**I**	
1	**2**	**3**	**4**	**5**	**6**	**7**
1605	41	1604	99	1603	50	ν(CC ring3)+δ(CH ring3)
1504	11	1502	39	1514	33	δ($C2H_2$)
1452	26	1468	51	1444	37	δ(CH_2, CH, NH)
1363	47	1358	66	1355	18	δ(CH_2, CH ring1)+δ($C11H_2$)
1288	20	1297	39	1285	40	ν(CC ring3)+δ(CH, CH_2 ring1)
1223	41	1218	92	1234	52	δ(CCC ring2)+τ(CH_2)

1198	31	1197	53	1178	45	ν(C13C14)+δ(CH ring2)+δ(C13H)
1	**2**	**3**	**4**	**5**	**6**	**7**
1140	71	1159	42	1168	22	$\tau(C2H_2)$+ν(C7O10)
1090	13	1094	27	1079	16	δ(OCC ring4)+δ(ring3, ring4)+ ν(C11C12)
1062	26	1063	21	1063	18	ν(CO ring4)+δ(CCC ring3)+ν(C11C7)
988	42	982	24	979	25	δ(CCC ring1)+ν(O2C11)
966	37	946	13	969	30	ν(CC ring1)+δ(CH, CH_2, NH ring1)
844	47	846	56	868	51	breathing(ring2)+δ(CH, CH_2, NH ring1)
812	67	805	100	835	100	breathing(ring3+ ring4)+δ(CH ring3)
715	22	720	35	734	54	ν(CO ring4)+ν(CC ring3)+$\delta(C2H_2)$
676	14	675	6	678	10	δ(ring1,3,4)+δ(O10C11C12)
631	28	635	35	650	39	ν(CC ring2)+δ(CH ring2)
584	17	573	21	583	24	δ(ring1, ring2, ring3)
535	19	522	11	524	18	δ(CCC ring1,2,3)+δ(C7O10C11)
478	18	470	11	476	18	δ(ring1)
347	19	351	35	343	91	γ(ring3, ring 4)+$\rho(C11H_2)$
		253	26	252	99	δ(ring1, ring2)
243	100					ν(AgO)+ν(AgN)

I_S-SERS intensity, I_R-Raman Intensity; I-Intensity, ν- stretch, ν_s- symmetric stretch, ν_{as}- asymmetric stretch, δ- in plane bending, ρ- rocking, τ-twisting, ω-wagging, γ-out of plane bending, ring1: piperidine ring (N22-C21-C12-C13-C24-C23); ring2: fluorophenyl ring (C14-C15-C16-C17-C18-C19); ring3: benzene ring (C4-C5-C6-C7-C8-C9); ring4: dioxolane ring (O1-C2-O3-C5-C4)

Orientation perpendicular to the silver surface piperidine ring (Fig. 4.5.) Is proved by intense SERS bands in the region 966-988 cm^{-1} due to stretching vibrations of the ring CC.

Intense SERS bands at 1363 and 1452 cm^{-1} are due to bending vibrations (deformation) plan groups CH_2, CH and NH piperidine ring.

4.5. Partial conclusions

Spectra recorded FTIR, FT-Raman and SERS of paroxetine were assigned based on DFT theoretical calculations. Very good correlation found between experimental and theoretical data is good evidence for the assignment of all vibrational bands as shown in table 4.

Based on SERS and Raman spectra analysis and considering MEP map of the molecules and SERS selection rules, it was determined that adsorption of paroxetine on silver nanoparticles is achieved by oxygen atoms (1, 3, 10) and nitrogen (22). Benzodioxol ring is adsorbed in a tilted orientation, right next to the silver surface, while the piperidine ring and the The benzenic are oriented perpendicular to the surface of silver.

5. SPECTROSCOPIC STUDY OF THE NEW KEGGIN POLYOXOMETALATES

5.1. General data of polyoxometalate

Polyoxometalates (POMs) are metal-oxygen clusters, presenting a fascinating variety of structures and properties, including size, shape, density, acidity, redox reaction, stability, solubility, etc.. Polioxometalații transition metal (substitute TMSPs) have attracted increased interest in the chemistry of polyoxometalates continuously being of great interest in catalysis, materials science and medicine [29].

A widespread means of functionalizing polyoxometalates [30] is the substitution of some of the addenda atoms with other elements. Substituting (Mo, W) with lower-valent atoms (V, Nb, Ta) has been deemed as interesting, as it leads to further oligomerization of the polyoxometalates into larger structures [31], or complexation with electrophilic moieties [32]. The Keggin [33] type anions, which are the most widely studied polyoxometalates, structural information on those substituted with lower-valent atoms are well established [33].

Monolacunary $[P^{v}VW_{10}O_{39}]^{8-}$ Keggin polyoxo-monovanado-decamolybdophosphate anion with mixed addenda form new complexes with transition metal cations, in which the metal-to-ligand ratio is 1:1. The aim of the present paper is to reports the synthesis and investigation of five new complexes of the $[P^{v}VW_{10}O_{39}]^{8-}$ ligand, with M^{n+} transition metal cations (Mn^{2+}, Fe^{3+}**,** Co^{2+}, Ni^{2+} and Cu^{2+}) with a Keggin structure and 1:1 molar ratio, which correspond to the general formula $K_{8-n}[M^{n+}(H_2O)PVMo_{10}O_{39}] \cdot xH_2O$. The complexes were

investigated and characterized by FT-IR, UV-Vis, EPR spectroscopy and powder X-ray diffraction. This allowed for the further determination of the behavior of the encapsulated transition metal ion, their coordination by the Keggin fragments, the corresponding local symmetry and their structure.

All chemicals were obtained from commercial sources and used without further purification. Distilled water was used for all procedures. Elemental analysis of P, Mo, V, Mn, Fe, Co, Ni and Cu was performed on a Varrian ASA 220 type spectrophotometer. Thermal stability analyses were performed in air on a Paulik-Erdely OD-103 derivatograph (20-800°C) at 5 ^{0}C min^{-1}. FTIR spectra were recorded in the 400-4000 cm^{-1} on a Biorad FTS 60A spectrophotometer using KBr pellets. FT-Raman spectra were performed on solid powders at room temperature, using a DILOR OMARS 89 Raman spectrophotometer (λ = 1064 nm). UV-VIS spectra were recorded in the 190-1100 nm on Shimadzu UV-VIS model mini-1240 spectophotometer. EPR spectra were obtained with a Bruker ESP 380 spectrometer. Powder XRD patterns were obtained with a Bruker D8 Advance powder diffractometer at 40kV and 40 mA, equipped with an incident beam Ge 111 monochromator using CuKα_1 radiation (λ = 1.540598 Å). The patterns were indexed using the Dicvol method [35].

5.2. Synthesis of new polyoxometalates

5.2.1. Synthesis of the monolacunary polyoxometalate ligand $K_8[PVMo_{10}O_{39}]\cdot 16H_2O$ (L)

To a solution obtained by dissolving 17.53 g (72.42 mmol) $Na_2MoO_4\cdot 2H_2O$ in 50 mL distilled water, 1.00 g (7.25 mmol) $NaH_2PO_4\cdot H_2O$ in minimum distilled water, and then 1.42 g (7.25 mmol) of $NaVO_3\cdot 2H_2O$ solved in minimum quantity of distilled water was added dropwise under stirring. The resulting solution was stirred for 30 minutes at room temperature. When the solution cleared, the pH was adjusted at 4.7 with 1 M HCl solution. Any insoluble material was removed by filtration under suction and 5.00 g (67 mmol) KCl was added to the red filtrate, after which the solution was kept at 5 ^{0}C for 30 minutes. Orange crystals of $K_8[PVMo_{10}O_{39}]\cdot 11H_2O$ were obtained, which were collected and washed with 20 mL deionized water, 20 mL ethanol and 20 mL diethyl ether and then dried in a desiccator. Yield: 6.85 g (43.6 %). UV (nm): 212; 310; IR (cm^{-1}): 3569 s, 3489 s, 3474 s, 3186, 1624 m, 1042 w, 1031 w, 984 m, 945 vs, 929 s, 839 m, 807 m, 729 m, 690 sh, 593 w, 523 w; Raman (cm^{-1}): 960 vs, 889 w, 505 w, 376 w, 229 m, 150 w; Anal. Calcd for $K_8[PVMo_{10}O_{39}]\cdot 11H_2O$: K, 14.26; Mo, 43.73; V, 2.32; P, 1.41; H_2O, 9.54. Found: K, 14.00; Mo, 43.50; V, 2.00; P, 1.50; H_2O, 9.74%.

5.2.2. **Synthesis of the $K_6[Mn(H_2O)PVMo_{10}O_{39})]\cdot 10\ H_2O$ complex (1)**

To a solution obtained by dissolving 5 g (2.30 mmol) $K_8[PVMo_{10}O_{39}] \cdot 11H_2O$ in 40 mL distilled water having pH = 4.3 by adding 1N HCl , a solution obtained by dissolving of 0.46 g (2.30 mmol) of $MnCl_2 \cdot 4H_2O$ dissolved in minimum quantity of distilled water was added drop-wise under stirring. The pH was adjusted between 3.75-4.00 with 0.1 M HCl and 5% solution of $KHCO_3$ respectively. The mixture was kept at room temperature, 30 minutes under stirring. Any insoluble material was removed by filtration under suction and then to the filtrate was added 2 g (26.8 mmol) of KCl power, and kept 2-3 days at 6°C. After 3 days the red-orange crystals of $K_6[Mn(PVMo_{10}O_{39})(H_2O)] \cdot 10H_2O$ were filtered and washed with ethanol. The crystals were kept two days at room temperature in a desiccator. The complex was recrystallized from deionized water with pH 3.75 – 4.00, at room temperature. Yield: 2.6 g (49 %). UV (nm): 217, 313,5 IR (cm^{-1}): 3564 m, 3378 m, 1616 m, 1079 sh, 1062 w, 1045 w, 945 sh, 932 s, 870 m, 782 m, 720 m, 680 m, 643 m, 522 w; Raman (cm^{-1}): 1095 w, 987 s, 885 w, 229 m; Anal. Calcd for $K_6[Mn(H_2O)PVMo_{10}O_{39}] \cdot 10H_2O$: K, 10.87; Mo, 44.59; V, 2.37; Mn, 2.55; P, 1.44; H_2O, 9.20. Found: K, 10.84; Mo, 44.72; V, 2.20; Mn, 2.47; P,1.43; H_2O, 9.875%.

5.2.3. Synthesis of the $K_5[Fe(H_2O)PVMo_{10}O_{39}] \cdot 8H_2O$ complex (2)

The synthetic procedure above was followed using 0.37 g (2.30 mmol) $FeCl_3$ instead of $MnCl_2 \cdot 4H_2O$. The addition of KCl (2 g) to the solution led to red-orange crystals of $K_5[Fe(PVMo_{10}O_{39})(H_2O)] \cdot 8H_2O$, which were filtered off and dried in desiccator. Yield: 2.85 g (60.15 %). UV (nm): 218, 312; IR (cm^{-1}): 3470 m, 1609 m, 1080 w, 1068 w, 1051 w, 944 s, 858 m, 776 vs, 593 w; Raman (cm^{-1}): 995 s, 975 sh, 233 m; Anal. Calcd for $K_5[Fe(PVMo_{10}O_{39})(H_2O)] \cdot 8H_2O$: K, 9.38; Mo, 46.18; V, 2.45; Fe, 2.69; P, 1.49; H_2O, 7.79. Found: K, 9.30; Mo, 46.31; V, 2.29; Fe, 2.58; P, 1.42; H_2O, 7.81%.

5.2.4. Synthesis of the $K_6[Co(H_2O)PVMo_{10}O_{39}]\ 22H_2O$ complex (3)

The synthetic procedure above was followed using 0.53 g (2.30 mmol) $CoCl_2 \cdot 6H_2O$ instead of $MnCl_2 \cdot 4H_2O$. The addition of KCl (2 g) to the solution led to red-orange crystals of $K_6[Co(PVMo_{10}O_{39})(H_2O)] \cdot 17H_2O$ which were filtered off and dried in desiccator. Yield: 2.61 g (51 %). UV (nm): 212, 315; IR (cm^{-1})3470 sh, 3373 m, 1617 m, 1080 w, 1068 w, 1051 w, 942 s, 887 m, 779 s, 520 w; Raman (cm^{-1}): 989 s, 974 s, 229 m; Anal. Calcd for $K_6[Co(PVMo_{10}O_{39})(H_2O)] \cdot 17H_2O$: K, 10.25; Mo, 42.05; V, 2.23; Co, 2.58; P, 1.36; H_2O, 14.19. Found: K, 10.08; Mo, 42.18; V, 2.15; Co, 2.46; P, 1.33; H_2O, 14.19%.

5.2.5. Synthesis of $K_6[Ni(H_2O)PVMo_{10}O_{39}] \cdot 21H_2O$ complex (4)

The synthetic procedure above was followed using 5.5 g (2.3 mmol) $NiCl_2 \cdot 6H_2O$ instead of $MnCl_2 \cdot 4H_2O$. The addition of KCl (2 g) to the solution led to

red-orange crystals of $K_6[Ni(H_2O)PVMo_{10}O_{39}]\cdot 21H_2O$ which were filtered off and dried in desiccator. Yield: 3.1 g (58 %). UV (nm): 214, 314; IR (cm^{-1}): 3569 sh, 3470 sh, 3373 m, 1616 m, 1080 sh, 1062 w, 1045 sh, 945 sh, 939 vs, 874 s, 788 vs, 645 w, 518 w, 225 w; Raman (cm^{-1}): 991 s, 975 sh, 235 m; Anal. Calcd for $K_6[Ni(PVMo_{10}O_{39})(H_2O)]\cdot 21H_2O$: K, 9.94; Mo, 40.77; V, 2.17; Ni, 2.49; P, 1.32; H_2O, 16.82. Found: K, 9.89; Mo, 40.89; V, 2.02; Ni, 2.41; P, 1.28; H_2O, 16.72%.

5.2.6 Synthesis of $K_6[Cu(H_2O)PVMo_{10}O_{39}]\cdot 17H_2O$ complex (5)

The synthetic procedure above was followed using 0.39 g (2.3 mmol) $CuCl_2\cdot 6H_2O$ instead of $MnCl_2\cdot 4H_2O$. The addition of KCl (2 g) to the solution led to red-orange crystals of $K_6[Cu(PVMo_{10}O_{39})(H_2O)]\cdot 17H_2O$ which were filtered off and dried in desiccator. Yield: 2.0 g (38 %). UV (nm): 211, 316; IR (cm^{-1}): 3569 sh, 3373 m, 1617 m, 1080 w, 1062 w, 1045 w, 941 s, 872 m, 782 s, 593 w, 520 sh; Raman (cm^{-1}): 996 sh, 979 vs, 519 w, 235 m, 156 w, 108 w; Anal. Calcd for $K_6[Cu(PVMo_{10}O_{39})(H_2O)]\cdot 17H_2O$: K, 10.23; Mo, 41.97; V, 2.23; Cu, 2.78; P, 1.36; H_2O, 14.16. Found: K, 10.20; Mo, 42.15; V, 2.18; Cu, 2.62; P, 1.33; H_2O 13.41%.

5.3. Results and discussions

The $K_8[PVMo_{10}O_{39}]\cdot 11H_2O$ ligand polyoxometalate, was synthesized at pH=4 by according to the following chemical reaction:

$$10Na_2MoO_4+NaH_2PO_4+NaVO_3+14HCl+8KCl = K_8[PVMo_{10}O_{39}]\cdot 11H_2O+22NaCl + 8H_2O$$

The $K_8[PVMo_{10}O_{39}]\cdot 11H_2O$ was investigated by chemical and thermo-gravimetrical analysis and by means of spectroscopic (FT-IR, UV) methods.

The 1:1 complexes, which correspond to the general formula $K_{(8-n)}[M^{n+}(H_2O)PVW_{10}O_{39}]\cdot xH_2O$, are obtained starting from α-$[PVW_{10}O_{39}]^{8-}$ as potassium salt and transition metals M^{n+} in molar ratio of 1: 1, at pH=3.8 - 4.0, according to the following reaction:

$$M^{n+} + [PVMo_{10}O_{39}]^{8-} + H_2O = [M^{n+}(H_2O)PVMo_{10}O_{39}]^{(8-n)-}$$

The isolation of the compounds **1-5** as potassium salts resulted in relatively good yields of the polyoxometalate complexes. The data from chemical and thermo-gravimetrical analysis are in good agreement with the proposal formulas for new compounds.

5.3.1. Thermal stability

The thermal stability of **1-5** complexes was investigated by TG-DTG-DTA. The weight loss between 20-175 ^{0}C corresponds to lattice water molecules content. The dehydration process is accompanied by two endothermic processes at ~70 ^{0}C and ~ 180 ^{0}C as

observed on the DTA curve. The second weight loss observed on the DTG curve between 270–350 ^{0}C is assigned to the loss of the coordination molecule. According to the literature, the first exothermic peak of DTA curve, which usually occurs at 20–30 ^{0}C after the temperature of polyoxometalate decomposing [46], is regarded as the thermal stability sign of polyoxometalates [47]. For the compounds **1-5,** the first exothermic peak appeared between 330 ^{0}C - 360 ^{0}C, indicating a good thermal stability of the complexes in following order:

L(276°C)<**5**(331°C)<**1**(345°C)<**2**(346.5°C)< **3**(348.5^{o}C)<**4**(351°C)

The endothermic processes at ~430 °C and ~540 °C are due to oxides mixture formation and structural transformations.

5.4 Vibrational spectral

5.4.1. FTIR spectra

The FTIR spectra of complexes **1-5** in the range of 4000-400 cm^{-1} are shown in Fig.5.1 along with those of the monolacunary Keggin ligand $K_8[PVMo_{10}O_{39}]\cdot 16H_2O$. By comparing the FT-IR frequencies of the monolacunary ligand **L** with those of the transition metal cation complexes **1-5**, we have obtained information concerning the coordination of the transition cations in the vacant position of the monolacunary polyoxometalate ligand. The similarities of FTIR spectra for ligand **L** and for complexes **1-5** show that the main vibration bands are due to the polyoxomolibdate structure [48].

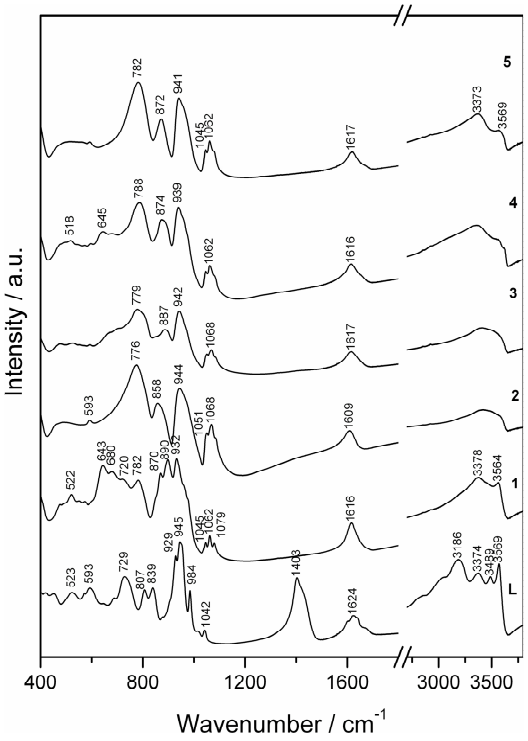

Fig. 5.1 FTIR spectra

In the FTIR spectrum of ligand **L** the intense broad band at ~ 3374 cm^{-1} is attributed to hydrogen-bonded ν_{as}(OH) vibration, and in–plane δ(OH) bending appears as a medium band at 1624 cm^{-1}. The shoulders on the very broad ν_{as}(OH) vibration band (3000-5570 cm^{-1} region) are due to the coexistence of the crystallization and coordinated water molecules. In spectra of the complexes, the intense broad vibration band, ν_{as}(OH), between 3570-3370 cm^{-1}, corresponds to the vibration stretching coordination water involved in hydrogen bonds and is due to the crystallization water, as well. The in-plane OH bending δ(OH) appears in complexes **1-5** as a medium band between 1609-1617 cm^{-1} involved in hydrogen bonds with neighboring water molecules [18]. The ν_{as}(P-O_i), where O_i is the internal oxygen atom which links P and mixed addenda of Mo and V, respectively, frequency appearing in the ligand **L** spectrum as two weak bands at 1042 cm^{-1} and 1031 cm^{-1}, while in complexes **1-5** spectra these appearing as three weak bands, showing the presence of phosphorus as heteroatom in the polyoxometalate framework. The tiny shift of the ν_{as}(P-O_i) anti-symmetric stretching vibrations towards higher energies in complexes **1-5** indicates that the coordination increases the cohesion of the monolacunary ligand structure around transition metal cations. The bands of the stretching vibration of the ν_{as}(Mo-O_t) and ν_{as}(V-O_t) in the ligand shown at 984 cm^{-1} and 945 cm^{-1}, respectively, are superposed in spectra of the complexes **1-5**, and shown as broad band between 932- 944 cm^{-1} [19]. The relative small shift of the ν_{as}(Mo-O_t) stretching vibrations, either towards lower frequencies (by 932 (s) for **1**, 944 (s) for **2**, 942 (s) for **3**, 939 (s) for **4** and 941 (s) for **5** cm^{-1}, respectively) is due to fact that the terminal O_t atoms are not involved in the co-ordination of the transition metal cations. The two bands at 929 (vs, sp) cm^{-1} and 839 (m) cm^{-1}, respectively, for tricentric Mo-O_c-Mo bonds of the corner-sharing MoO_6 octahedra, are shown in the spectrum of the ligand and only one medium band appears in FT-IR spectra of the complexes (by 870 for **1**, 858 for **2**, 887 for **3**, 874 for **4** and 872 for **5**, respectively). The increase in the spectra of the complexes the ν_{as}(Mo-O_c-Mo) frequency for the tricentric bonds of corner-sharing that belongs to the cap region indicates the shortening of these bonds after the metallic ions complexation. Similarly, two vibration bands for tricentric Mo-O_e-Mo bonds of the edge-sharing MoO_6 octahedral appear in the FTIR spectra of the ligand at 807 (w) cm^{-1} and 729 (m) cm^{-1}, respectively, suggesting that two nonequivalent bonding of this type are present. In complexes **1-5** one of them belonging to the belt region lost, but the other belonging to the cap region with the lower frequency remains (by 782 (vs) for **1**, 776 (vs) for **2**, 779 (s) **3**, 788 (s) for **4** and 782 (vs) for **5** cm^{-1}, respectively). The increase in the spectra of the complexes of the νas(Mo-O_e-Mo) frequencies for the tricentric

bonds of edge-sharing MoO_6 octahedral indicates the shortening of these bonds after the metallic ion complexation and increase the symmetry and stability of these compounds. In conclusions can to say that the shift of ν_{as}(Mo-O_c-Mo) and ν_{as}(Mo-O_e-Mo) frequencies for the bonds from the cap region of the monovacant Keggin units, shows the coordination of each transition metallic ion by the oxygen atoms from corner-sharing and edge-sharing octahedral.

5.4.2. The FT-Raman spectra

The FT-Raman spectra of complexes **1-5** in the 1200-100 cm^{-1} are shown in Fig.5. 2 comparatively with those of the monolacunary Keggin ligand $K_8[PVMo_{10}O_{39}]$ $\cdot 16H_2O$.

.

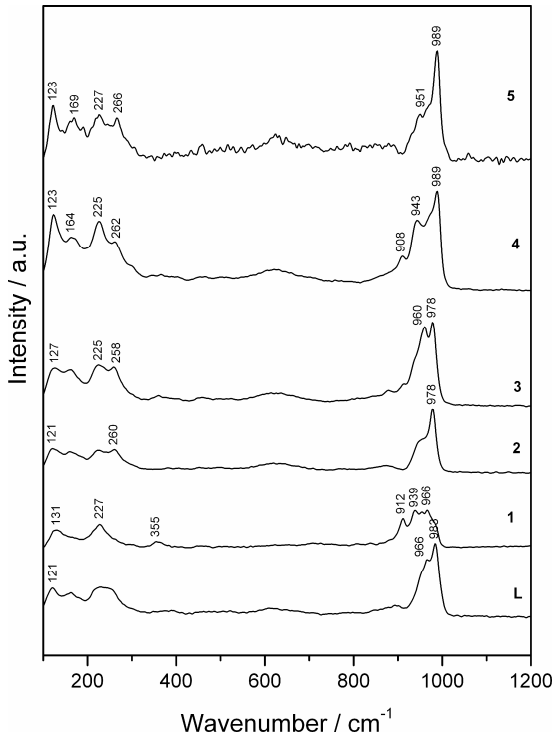

Fig. 5.2 **FT-Raman spectra**

The Raman spectrum of the ligand shows the three characteristic bands at 960 (vs) cm^{-1}, 889 (m) cm^{-1} and 229 (m) cm^{-1}, assigned to ν_s(Mo-O_t), ν_{as}(Mo-O_t) and ν_s(Mo-O_i), respectively. These bands are shifted in the FT-Raman spectra of the complexes (at 987 (s), 885(sh) and 229 (w) cm^{-1} for **1**, 995 (s), 975 (sh) and 233 (w) cm^{-1} for **2**, 989 (s), 974 (s) and 229 (w) cm^{-1} for **3**, 991 (s), 975 (sh) and 235 (w) cm^{-1} for **4**, and 996 (sh), 979 (vs) and 235 (m) cm^{-1} for **5**, respectively). In the FT-Raman spectra, the bands assigned to vibrations of the complexes **1-5**, Mo-O_t bonds were shifted towards higher energies, comparatively with the ligand. This suggests higher stability of the complexes [34].

5.4.3. Electronic Spectra

We have registered the electronic UV and Vis spectra on aqueous solutions of the potassium salts of the complexes **1-5** and compared them with that of the ligand or with that of hexaaqua complexes of the Mn^{2+}, Fe^{3+}, Co^{2+}, Ni^{2+} and Cu^{2+} in octahedral field [35].

5.4.4. UV-Spectra

UV spectra of polyoxometalate clusters generally exhibit two charge-transfer (CT) bands, characteristic to the polyoxoanionic framework, which are ascribed to oxygen-to-metal transitions. In UV spectrum of the ligand **L,** the broad ν_1 CT band, due to dπ-pπ-dπ transitions from the tricentric Mo-$O_{c,e}$-Mo and Mo-$O_{c,e}$-V bonds recorded at 321 nm/31150 cm^{-1}. The sharper ν_2 CT band, due to dπ-pπ transitions of the Mo=O_t and V=O_t bonds, have the maximum detected at 209 nm/47850 cm^{-1}. The UV spectra of the ligand and complexes are also similar, proving that the charge transfer inside in polyoxometalate structure is not significantly affected by coordination. The lower energy band ν_1 was shifted to higher frequencies in complexes spectra, compared to the ligand, and this is due to the increase of the symmetry, of the MoO_6 and VO_6 octahedra through complexation, which influences the electronic transfer from these bonds. The higher energy band ν_2 was shifted to lower frequencies in complexes spectra, compared to the ligand, and this is due to the decrease of the symmetry, of the MoO_6 and VO_6 octahedra through complexation, which influences the electronic transfer from these bonds

5.4.5. Visible-Spectra

Visible spectra only show electron transfer bands of the M^{n+} transition metal ions coordinated by the ligand.However, the expected transition bands are not found in the spectrum of complex **1** and **2**. The very low intensity d-d transitions of the (d^5) Fe^{3+} and Mn^{2+} ions, forbidden by the Laporte and spin selection rules, are totally masked by the ν_1 charge transfer band, which extends from UV into the visible range [35]. This indicates that Fe^{3+} and Mn^{2+} ions are involved in the charge transfer in complexes **1** and **2.**

The absorption bands of the **3-5** complexes recorded in the visible range (nm/cm^{-1}), were compared to those of the corresponding $Co(H_2O)_6^{2+}$, $Ni(H_2O)_6^{2+}$ and $Cu(H_2O)_6^{2+}$ aqua-cations in octahedral field conform to literature [21]. The Vis spectrum of complex **3** (Fig.5.3) shows the characteristic features of Co^{2+} (d^7) ion in a distorted octahedral environment: show two bands at 575 nm/17390 cm^{-1} and 940 nm/10630 cm^{-1} corresponding to the $^3A_{2g}(F) \rightarrow {}^3T_{1g}(F)$ (ν_2) and $^4T_{1g}(F) \rightarrow {}^4T_{2g}(F)$ (ν_1) transitions

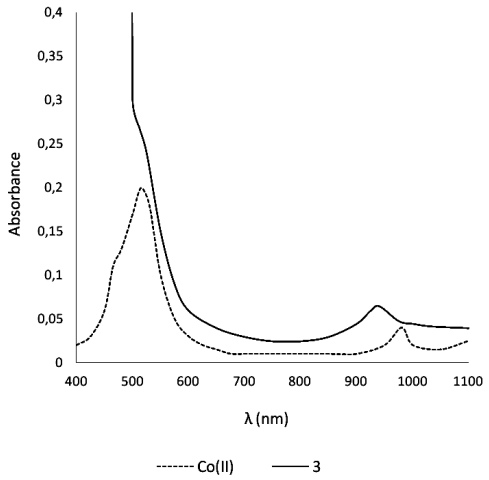

Fig. 5.3 Visible spectrum of the complex Co(II)

The Vis spectrum of complex **4 (**Fig.5. 4) shows the characteristic features of Ni^{2+} (d^8) ion in a distorted octahedral environment: show two bands at 702 nm/13950 cm^{-1} and 795 nm/12950 cm^{-1} corresponding to the $^3A_{2g}(F) \rightarrow {}^3T_{1g}(F)$ (ν_2) and $^3A_{2g}(F) \rightarrow {}^3T_{1g}(P)$ (ν_3) transitions.

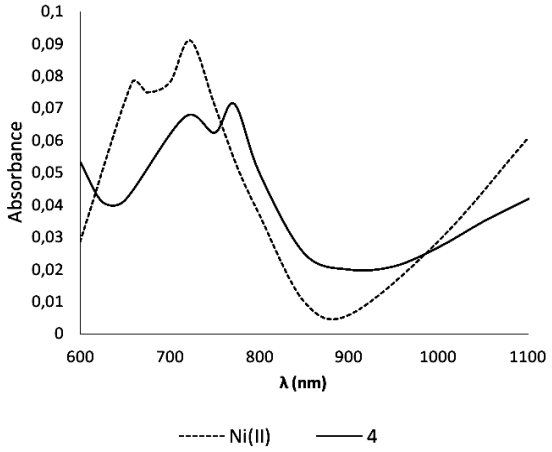

Fig. 5.4 Visible spectrum of the complex Ni(II)

The visible spectrum of the complex **5** (Fig. 5.5) presents a broad absorption centered at approximately 858 nm/11650 cm^{-1} suggesting a distorted octahedral environment around the Cu^{2+} (d^9) ion. This band can be attributed to the $^2E_g \rightarrow {}^2T_{2g}$ transition. Three transition are expected (d_{xy}, $d_{yz} \rightarrow d_x^2$ and $d_{xy} \rightarrow d_{x^2-y^2}$), but these are very close in energy and give rise to a single asymmetric broad band.

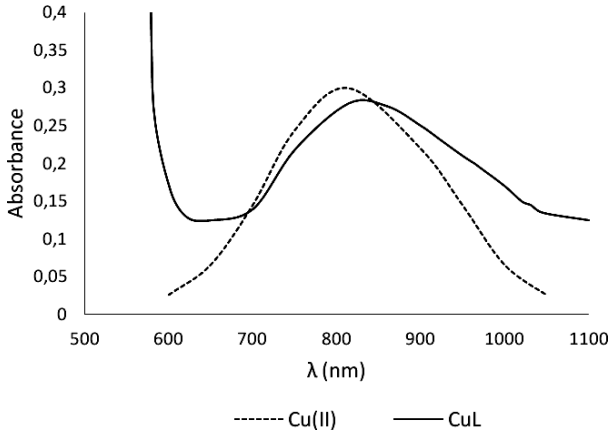

Fig. 5.5. Visible spectrum of the complex Cu(II)

The greater shift in the case of the copper ion in the complex **5**, as opposed to the aqua copper complex associated with the band assymmetry can be traced back to the Jahn-Teller distorsion.

5.4.6. Spectrum ESR

EPR signals are due to the presence of the paramagnetic transition metal ions. Some EPR spectra are presented down.

EPR spectrum of compound **2** (Fig.5. 6) contains signals at g_1=7.942, g_2=4.265 and g_3=1.997 specific for Fe^{3+} ions. The hyperfine lines for the vanadium ion with axial symmetry were solved in g=2 *area*

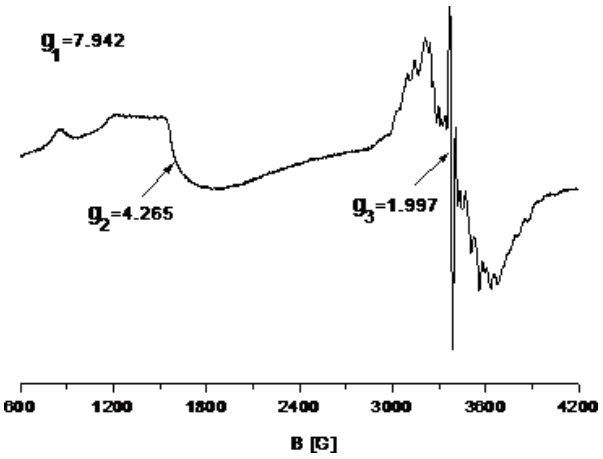

Fig. 5.6. Spectrum ESR of compound 2

Four metallic hyperfine lines for monomeric copper(II) were resolved, both in parallel and in perpendicular bands are included in the EPR spectrum (***Fig. 5.7***).

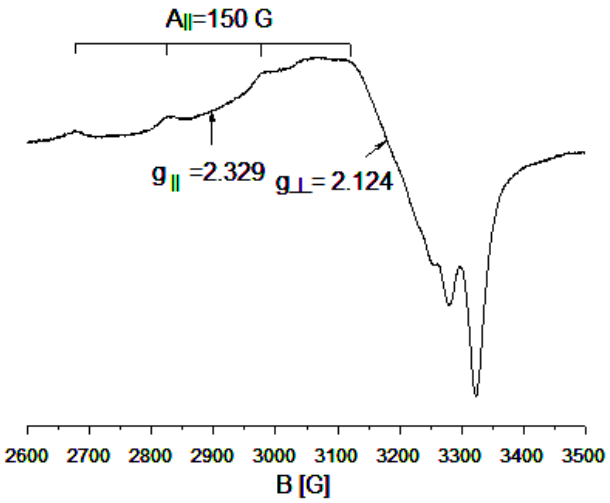

Fig. 5.7. Spectrum EPR

The powder EPR spectra obtained in the X band at room temperature are typical for octahedral mononuclear species.

5.5. Partial Conclusions

This work reports the synthesis and characterization of the potassium salt of the monosubstituted α-Keggin monovanado-decamolybdo-phosphate with Mn^{2+}, Fe^{3+}, Co^{2+}, Ni^{2+} and Cu^{2+} cations, a very interesting category of compounds, because of the catalytic and biologic properties of the vanadium element.

The complexes were synthesized in aqueous solution, by the direct addition of transition metal cations to a solution of the monolacunary Keggin polyoxo-monovanado-decamolybdo-phosphate anion. Elemental analysis is in good agreement with calculated values for general formula of $K_{8-n}[M^{n+}(H_2O)PVMo_{10}O_{39}]\cdot xH_2O$**.**

The IR spectra show that the $K_8[PVMo_{10}O_{39}]\cdot 16H_2O$ act as pentadentate ligand with octahedral coordination involving the oxygen atoms from corner-sharing and edge-sharing octahedral of monolacunary cavity and the oxygen atom from one water coordination molecule.

Visible electronic and EPR spectra indicate O_h local symmetry for transition metal cations in studied compounds

Conclusions

New synthesized metal complexes were so far unreported in the literature and characterized in terms of physicochemical and spectroscopic.

Given their bioaplicabilitatea were synthesized and characterized as some artificial cores of metal ion complexes Cu^{2+} : Cu (5 - etil –[1, 3, 4] – thyadiazol -2 -)$_2$ ($C_{12}H_8N_2$) (H_2O) şi Cu_2(5 - etil –[1, 3, 4] – thyadiazol -2 -) $(OH)_2$ (C_3H_7NO) (H_2O)] (H_2O) with sulfonamidic. These ligand complex reactions occur particularly free radicals can separate DNA molecule.

Research should aim for these complexes is developing new biological tools for studying DNA, development of potential anticancer or antiviral agents.

Very good concordance between experimental spectra of FTIR, FT-Raman and SERS of paroxetine with those obtained from DFT theoretical calculations show a very good optimization of molecular geometry.

Based on SERS and Raman spectra analysis and considering MEP map of the molecules and SERS selection rules, it was determined that paroxetine molecule adsorption on the surface of silver nanoparticles is achieved by oxygen atoms O1, O3, O10 and N22 nitrogen. Benzodioxol ring is absorbed in an inclined orientation, right next to the silver surface, while the piperidine ring and the.The benzenic are oriented perpendicular to the surface of silver.

Visible electronic spectra are characteristic of transitional elements, which functions as the central heteoatomi complexes, with their octahedral symmetry were determined transition ions.

Analytical results are in good agreement with the compositions calculated from chemical and physical formulas proposed.

In case the five new type polyoxometalate α-Keggin with the general formula $K_{(8-n)}[M^{n+}(H_2O)PVW_{10}O_{39}] \cdot xH_2O$,where M^{n+}= Mn^{2+}, Fe^{3+}, Co^{2+}, Ni^2 Cu^{2+}, synthesized in water solutions elemental analysis confirms the stoichiometry of the complexes. They are a very interesting class of compounds because of catalytic and biological properties of the element vanadium.

Complexes were synthesized in water solution by direct addition of transition metal cations Keggin in solution monolacunară polyoxo-monovanado-decamolibdo-phosphate anion. Elemental analysis is in good agreement with the values calculated for the general formula of $K_{8-n}[M^{n+}(H_2O)PVMo_{10}O_{39}]\cdot xH_2O$.

FT-IR spectra of the complexes studied are observed strong shift vibration frequencies corresponding links Mo-$O_{c,e}$-Mo and how pentadentat octahedral ligand with coordination involving oxygen atoms and the exchange of information and sharing octahedral cavity of an atom monolacunare oxygen from a water molecule.

The results confirm further research both in terms of biological activity of these compounds and their use in various areas reminding medicine, pharmacy, food and chemical industry.

Selective bibliography

1. R. Bentlez, *Biochemistry and Molecular Biology Edication*, 2005 p. 33-250.

2. R. Power, H.K. ,*Biological chemistry and absorption of inorganic and organic metals* ,European Bioscience Centre ,Ireland 2000

3. Gh. Marcu, M. Rusu, *" Polyoxometalate Chemistry ",* Ed. Tehnică*, 1997*

4. M.T. Pope, *"Polyoxoanions" in Encyclopedia of Inorganic Chemistry, R.B. King Ed., John Willey & Sons, Chichester, England, 1994, p. 3361-3371*

5. C.Hill,*Polyoxometalates* ,Ed:Chemical Revieww American Chem.Society ,Washington (1999)

6. K. Burger*, Coordination Chemistry: Experimental Methods,* Akademiai Kiado, Budapesta, 1973.

7. D. Williams*, The metals of life: the solution chemistry of metal ions in biological systems;* Van Notrand Reinhold Company: London, New York, 1971.

8. H. Neacsu, L. Jantschi*, Analytical Chemistry and Instrumental,* Academic Pres & Academic Direct, 2006.

9. J.L. Garcia-Gimenez, M. Gonzalez-Alvarez, M. Liu-Gonzalez, B. Marcias, J. Borras, G. Alzuet, J. *Inorg. Biochem.* 103, (2009) 243.

10. P.S. Mdluli, N.M. Sosibo, N. Revrapasadu, P. Karamanis, J. Leszczynski*, J. Mol. Struct*. 935 (2009) 32.

11. M. Moskovits, J.S. Suh, J. *Phys. Chem*. 88 (1984) 5526.

12. I. B. Cozar, L. Szabo, N. Leopold, V. Chiş, O. Cozar, L. David, *J. Molec. Struct*. 993 (2011) 308.

13. M. Baia, S. Astilean, T. Iliescu, *Raman and SERS Investigations of Pharmaceuticals*, Springer-Verlag, Berlin, 2008.

14. L. David, O. Cozar, C. Cristea, L. Gaina, *Identification of the molecular structure by spectroscopic methods,* Ed. Presa Universitară Clujeană, 2002

15. N. Leopold, *Surface Enhanced Raman Spectroscopy – Selected Applications*, Ed. Napoca Star, 2009.

16. I.B. Cozar, L. Szabo, N. Leopold, **D. Mare**, V. Chiş, L. David, Vibrational spectroscopic and DFT study of paroxetine, 30th European Congress on Molecular Spectroscopy, Florence, 29 Aug. – 3 Sept. 2010, p.303

17. L. Szabó, V. Chis, A. Pîrnău, N. Leopold, O. Cozar, S.z. Orosz, J. Mol. Struct. 924– 926 (2009) 361.

18. S.J. Mathew, R.B. Price, D.C. Shungu, X. Mao, E.L.P. Smith, J.M. Amiel, J.D. Coplan, J. Psychopharmacol. 24 (2010) 1175.

19. J.K. Aronson, Meyler's Side Effects of Drugs: The International Encyclopedia of Adverse Drug Reactions and Interactions, 2006, pp. 2722–2725.

20. M. Urbanova, V. Setnicka, P. Bour, H. Navratilova, K. Volka, Biopolymers 67 (4– 5) (2002) 298.

21. I.B. Cozar, L. Szabo, **D. Mare**, N. Leopold, L. David, V. Chiş, J. Molec. Struct. 993 (2011) 243.

22. S.E.J. Bell, N.M.S. Sirimuthu, Chem. Soc. Rev. 37 (2008) 1012.

23. S. Cavalu, S. Cîntă-Pînzaru, N. Leopold, W. Kiefer, Biopolym. – Biospectrosc. 62 (2001) 341.

24. R.G. Parr, W. Yang, *Density-functional Theory of Atoms and Molecules*, Oxford University Press, New York, 1989.

25. C. Lee, W. Yang, R.G. Parr, Phys. Rev. B 37 (1998) 85.

26. N. Belai, M.T. Pope, *Chem. Commun.,* 5760 (2005).

27. Z. Kang, C.H.A. Tsang, Z. Zhang, M. Zhang, N. Wong, J.A. Zapien, Y. Shan, S.T. Lee, *J. Am. Chem. Soc.*, 17, 5326 (2007).

28. A. Muller, F. Peters, M.T. Pope, D. Gatteschi, *Chem. Rev.*, 98, 239 (1998).

29. M. Pope, A. Muller, "*From Platonic Solids to Anti-Retroviral Activity*", Kluwer Academic Publishers, Dordrecht, 1994.

30. A. Muller, F. Peters, M.T. Pope, D. Gatteschi, *Chem. Rev.,* 98, 239 (1998).

31. K. C. Kim, M.T. Pope, *J. Chem. Soc. Dalton Trans.,* 986 (2001).

32. H. Naruke, T. Yamase, B*ull. Soc. Jpn*., 75, 1275 (2002).

33. G. Xue, J. Vaissermann, P. Gouzerh, *J. Cluster Sci.,* 3, 405 (2002).

34. G. Socrates, "*Infrared and Raman Characteristic, Group Frequencies: Tables and Charts",* third edition, Wiley, Chichester, 2001.

35. M.S. Masond, O.H. Abd El-Hamid, *Transit. Met. Chem.*, 14, 233 (1989).

36. A.R. Tomsa, L. Muresan, A. Koutsodimou, P. Falaras, M. Rusu, *Polyhedron*, 22, 2901(2003).

37. Gaussian 98, revision A.11.3, M.J. Frisch J. Pople et. al., Gaussian Inc., Pittsburgh PA, **2002**.